ADVANCED MATERIALS

ment effect at the higher energy side more easily than quantum wires, we expect the SiNTs to be more useful for future optoelectronic devices.

Experimental

Porous alumina templates were prepared by an anodization process. An aluminum foil (99.99 %, 0.13 mm thick, Aldrich) was electropolished in a perchloric acid/ethanol solution (ethanol (95 vol.-%)/perchloric acid (70 vol.-%) = 5:1) at 9 °C at a constant dc (direct current) voltage of 18 V for 1.5 min. This cleaned aluminum sheet was then anodized in a 0.3 M oxalic acid solution at 5 °C at a constant applied voltage of 40 V for 6 h. The resultant aluminum oxide layer was removed by dipping into an aqueous mixture of phosphoric acid (6 wt.-%) and chromic acid (1.8 wt.-%) at 60 °C. The second anodization was performed for 20 min at the same conditions in order to form a regular pore array of hexagons. After pore widening by dipping into an aqueous solution of 0.1 M phosphoric acid for 10 min, we performed heat treatment to enhance the crystallinity of the alumina templates at 500 °C for 30 min under Ar atmosphere. A regular array of hexagonal porous alumina was formed on both surfaces of aluminum film. This template was brought into the MBE chamber to grow SiNTs, where the chamber was evacuated to a pressure of 5×10^{-10} torr. The Si atoms/clusters were supplied for 10 min by electron-beam evaporator with a growth rate of 0.07 Å s^{-1}. The substrate temperature was maintained at 400 °C in order to prevent the aluminum layer from being melted. After growth, the sample was further heat treated at 600 °C or 750 °C under ambient conditions for oxidation.

The morphology of the SiNTs was observed by the field-emission scanning electron microscope (FESEM, JEOL-JSM6770F). High-resolution transmission electron microscopy (HRTEM, JEOL-JEM3011, 300 keV) was also used to determine the atomic details of the SiNTs. For HRTEM observations, small pieces of SiNTs were peeled off from the alumina surface and suspended, followed by further dispersion in isopropanol simply by stirring and sonication. The solvent containing the SiNTs was dropped on a holey carbon micro-grid. The photoluminescence (PL) spectra were measured with a He–Cd laser (325 nm). The laser beam diameter was about 0.3 mm with a power of 10 mW.

Received: January 23, 2003
Final version: April 4, 2003

[1] S. Iijima, T. Ichibashi, *Nature* **1993**, *363*, 603.
[2] X. Duan, Y. Huang, Y. Cui, J. Wang, C. M. Lieber, *Nature* **2001**, *409*, 66.
[3] R. F. Service, *Science* **1998**, *281*, 940.
[4] J. Hu, M. Ouyang, P. Yang, C. M. Lieber, *Nature* **1999**, *399*, 48.
[5] U. Landman, R. N. Barnett, A. G. Scherbakov, P. Avouris, *Phys. Rev. Lett.* **2000**, *85*, 1958.
[6] S. Shingubara, O. Okino, Y. Sayama, H. Sakaue, T. Takahagi, *Solid State Electron.* **1999**, *43*, 1143.
[7] B. Marsen, K. Sattler, *Phys. Rev. B: Condens. Matter* **1999**, *60*, 11 593.
[8] S. B. Fagan, R. J. Barierle, R. Mota, A. J. R. Da Silva, A. Fazzio, *Phys. Rev. B: Condens. Matter* **2000**, *61*, 9994.
[9] G. Seifert, T. Köhler, H. M. Urbassek, E. Hernández, T. Frauenheim, *Phys. Rev. B: Condens. Matter* **2001**, *64*, 193 409.
[10] R. Q. Zhang, S. T. Lee, C. K. Law, W. K. Li, B. K. Teo, *Chem. Phys. Lett.* **2001**, *364*, 251.
[11] J. Sha, J. Niu, X. Ma, J. Xu, X. Zhang, Q. Yang, D. Yang, *Adv. Mater.* **2002**, *14*, 17.
[12] T. Kyotani, L. Tsai, A. Tomita, *Chem. Mater.* **1996**, *8*, 2109.
[13] T. K. Whidden, P. Thanikasalam, M. J. Rack, D. K. Ferry, *J. Vac. Sci. Technol. B* **1995**, *13*, 1618.
[14] Z. G. Bai, D. P. Yu, J. J. Wang, Y. H. Zou, W. Qian, J. S. Fu, S. Q. Feng, J. Xu, L. P. You, *Mater. Sci. Eng. B* **2000**, *72*, 117.
[15] Y. P. Varshni, *Physica* **1969**, *39*, 149.
[16] B. S. Kim, M. A. Islam, L. E. Brus, I. P. Herman, *J. Appl. Phys.* **2001**, *89*, 8127.
[17] C. Single, F. Zhou, H. Heidemeyer, F. E. Prins, D. P. Kern, E. Plies, *J. Vac. Sci. Technol. B* **1998**, *16*, 3938.
[18] H. Z. Song, X. M. Bao, N. S. Li, X. L. Wu, *Appl. Phys. Lett.* **1998**, *72*, 356.
[19] G. G. Qin, X. S. Liu, S. Y. Ma, J. Lin, G. Q. Yao, X. Y. Lin, K. X. Lin, *Phys. Rev. B: Condens. Matter* **1997**, *55*, 19.
[20] A. G. Cullis, L. T. Canhan, P. D. J. Calcott, *J. Appl. Phys.* **1997**, *82*, 909.

Strongly Polarized and Efficient Blue Organic Light-Emitting Diodes Using Monodisperse Glassy Nematic Oligo(fluorene)s**

By *Sean W. Culligan*, *Yanhou Geng*, *Shaw H. Chen*,* *Kevin Klubek*, *Kathleen M. Vaeth*, and *Ching W. Tang*

Conjugated polymers have been intensively explored for electronics, photonics, and optics over the past two decades by taking advantage of the diverse structures and properties made available through molecular design and synthesis.[1] A variety of device concepts have been demonstrated, such as organic light-emitting diodes (OLEDs),[2] organic lasers,[3] thin film transistors,[4] photoconductors,[5] and nonlinear optical devices.[6] Polymers that can be spin-cast into large-area thin films represent a material class complementary to low molecular mass materials that can be vacuum deposited[7] for LEDs. Recent studies have unraveled how photophysical properties of conjugated polymer films can be affected by interchain interactions and nanoscale morphology that are kinetically locked-in during the spin-coating process,[8] causing temporal instability of emission spectra because of π-stacking. To a large extent, this problem has been overcome by incorporating spiro-configuration, dendritic substitution, exciton migration, or end-capping into the molecular structure.[9,10] Potentially useful as an efficient light source for liquid crystal displays, linear[10–14] as well as cross-linked[15,16] nematic poly(fluorene) s have been actively pursued for polarized electroluminescence (EL). The uniaxial alignment of the conjugated backbones, which is imperative to polarized light emission, has been accomplished by thermally annealing a poly(fluorene) film on a conductive alignment layer. The required annealing temperature and time increase to 200 °C and a few hours, respectively, with an increasing molecular weight. For the preparation of a conductive alignment layer, varied approaches have been attempted, such as uniaxially rubbing a

[*] Prof. S. H. Chen, S. W. Culligan, Dr. Y. Geng
Department of Chemical Engineering
Center for Optoelectronics and Imaging, University of Rochester
240 East River Road, Rochester, NY 14623-1212 (USA)
Prof. S. H. Chen
Laboratory for Laser Energetics
250 East River Road, Rochester, NY 14623-1299 (USA)
E-mail: shch@lle.rochester.edu
K. Klubek, Dr. C. W. Tang
Hard Copy and Display Technology Division, Eastman Kodak Company
Rochester, NY 14650-2116 (USA)
Dr. K. M. Vaeth
Imaging Materials Division, Eastman Kodak Company
1999 Lake Avenue, Rochester, NY 14650-2116 (USA)

[**] The authors are grateful for the financial support provided by the Multidisciplinary University Research Initiative, administered by the Army Research Office, under DAAD19-01-1-0676, the National Science Foundation under Grant CTS-0204827, Eastman Kodak Company, and the New York State Center for Electronic Imaging Systems. Additional funding was provided by the Department of Energy Office of Inertial Confinement Fusion under Cooperative Agreement No. DE-FC03-92SF19460 with the Laboratory for Laser Energetics and the New York State Energy Research and Development Authority. The support of DOE does not constitute an endorsement by DOE of the views expressed in this article.

  DOI: 10.1002/adma.200304972

spin-cast polyimide film with or without a hole conductor as a dopant,[10–12,15] poly(*p*-phenylenevinylene),[14,15] or a complex consisting of poly(3,4-ethylenedioxythiophene) and polystyrene sulfonic acid, PEDOT/PSS.[17] A non-contact photoalignment layer doped with a hole conductor appears to be an attractive alternative.[13,16] An advantage of the PEDOT/PSS approach is the prevention of phase separation encountered with doped alignment layers.[18] Efficient unpolarized polymer light-emitting diodes have also been constructed with PEDOT/PSS as a hole injection and transport layer.[19]

As a class of photonic materials, monodisperse conjugated oligomers are characterized by a relatively short and uniform chain length, solubility and chemical purity, and ease of processing[20] with a potential for spontaneous uniaxial alignment mediated by nematic mesomorphism. Few existing conjugated oligomers are capable of forming glassy nematic films for polarized light emission with the exception of properly functionalized oligo(fluorene)s.[21] The potential of this material class has also been substantially enhanced with elevated glass transition and clearing temperatures while avoiding spontaneous crystallization normally encountered with low molecular mass organic materials. Here, we report the first polarized OLEDs using monodisperse oligo(fluorene)s on a PEDOT/PSS conductive alignment layer. These devices exhibit deep blue emission with a peak dichroic ratio of up to 31.2, an integrated dichroic ratio of up to 24.6, and a luminance yield of up to 1.10 cd A^{-1} without polarization analysis, representing the best set of performance data reported to date.

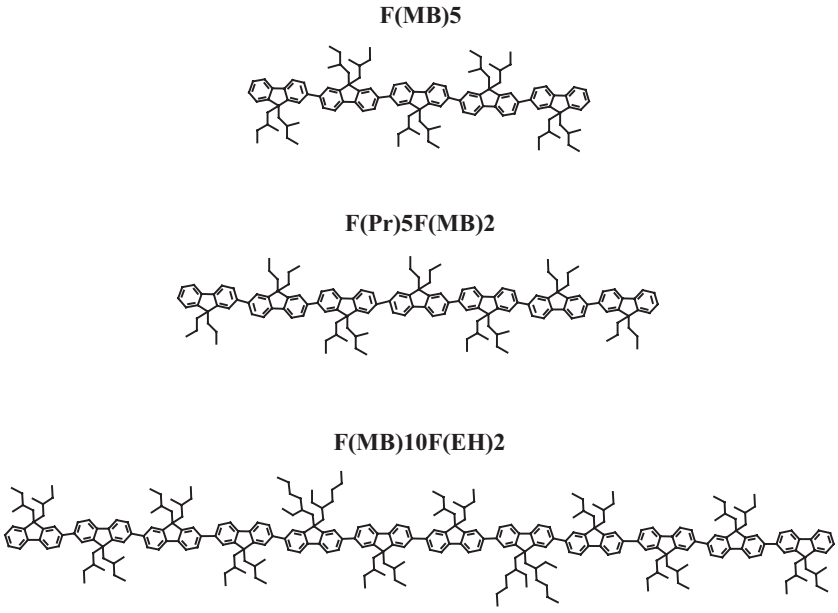

Fig. 1. Molecular structures with abbreviations of the three oligo(fluorene)s used in the present study.

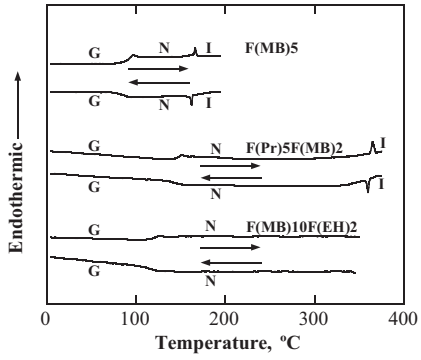

Fig. 2. The DSC heating and cooling thermograms at ±20 °C min^{-1} of samples preheated to 350 °C without thermal decomposition followed by cooling at –20 °C min^{-1} to –30 °C. Symbols: G, glassy; N, nematic; I, isotropic.

In a recent paper, we have reported a series of monodisperse oligo(fluorene)s with the objective of identifying structural parameters conducive to the formation of monodomain glassy nematic films via spin-coating on a polyimide alignment layer.[21] It was found that the oligomer's chain length, pendant structure, and molecular aspect ratio affect thermotropic properties, phase transition temperatures, glass-forming ability, and absorption and photoluminescence dichroic ratios. Three promising oligo(fluorene)s were selected for an exploration of polarized OLEDs, viz. penta[9,9-bis(2-methylbutyl)fluorene] (**F(MB)5**), 2,7-bis[9,9-bis(2-methylbutyl)-9′,9′,9″,9″-tetrakis(*n*-propyl)-7,2′;7′,2″-terfluoren-2-yl]-9,9-bis(*n*-propyl)fluorene (**F(Pr)5F(MB)2**), and 2,7′-bis[9,9-bis(2-ethylhexyl)-9′,9′,-9″,9″,-9″,9″,9‴,9‴-octakis(2-methylbutyl)-7,2′;7′,2″;7″,2‴;7‴,2⁗-pentafluoren-2-yl]-9,9,9′,9′-tetrakis(2-methylbutyl)-7,2′-bifluorene (**F(MB)10F(EH)2**), as depicted in Figure 1, where the pendant structures have been optimized with respect to the chain length to realize glassy nematic films.

Shown in Figure 2 are the differential scanning calorimetry (DSC) thermograms at a heating/cooling rate of ±20 °C min^{-1} of samples that had been preheated to 350 °C without thermal decomposition followed by cooling to –30 °C, revealing an absence of crystalline melting or crystallization as corroborated by hot-stage polarizing optical microscopy. While **F(Pr)5F(MB)2** was found to be thermally stable up to 380 °C, **F(MB)10F(EH)2** showed nematic mesomorphism up to 360 °C where thermal decomposition occurred. It is evident that a longer conjugated backbone contributes to a higher nematic-to-isotropic transition temperature, T_c, and a broader nematic fluid temperature range. The glass transition temperature, T_g, increases from **F(MB)5**, a pentamer, to **F(Pr)5F(MB)2**, an heptamer, but it is depressed by the bulky 2-ethylhexyl pendant to **F(MB)10F(EH)2**, a dodecamer, relative to **F(Pr)5F(MB)2**. The elevated T_g and T_c exhibited by all three oligo(fluorene)s are desirable for device application.

Neat oligo(fluorene) films were prepared by spin-coating from a UV-grade chloroform solution onto fused silica substrates with a buffed PEDOT/PSS conductive alignment layer. Upon drying under vacuum at room temperature, the oli-

ADVANCED MATERIALS

go(fluorene) film was annealed at 10 °C above its T_g for a period of 30–60 min, followed by cooling to room temperature at 5 °C min^{-1} in most cases to arrive at monodomain films. Sufficient annealing time was allowed to reach an asymptotic value in orientational order parameter, $S_{ab} = (R_{ab} - 1)/(R_{ab} + 2)$, in which the dichroic ratio, $R_{ab} = A_{\parallel}/A_{\perp}$, is the absorbance parallel over that perpendicular to the nematic director, as defined by the buffing direction on the PEDOT/PSS alignment layer. In general, a longer annealing time was required for a longer oligo(fluorene) or a thicker film. The monodomain character of the resultant glassy nematic films was ascertained by i) polarizing optical microscopy to be textureless but optically anisotropic, and ii) electron diffractometry to be non-crystalline (see the inset in Fig. 3a). The thickness of the conductive alignment layer and that of the oligo(fluorene) film were measured by variable angle spectroscopic ellipsometry following literature procedures.[22] As shown in Figure 3a for a 73 nm thick **F(MB)10F(EH)2** film, $S_{ab} = 0.82$ emerged from UV-vis linear dichroism, indicating a high degree of uniaxial alignment. Polarized photoluminescence of the same film is also presented in Figure 3a in terms of the emission intensity parallel ($PL_{\parallel}$) and perpendicular ($PL_{\perp}$) to the nematic director. The photoluminescence dichroic ratio, $R_{PL} = PL_{\parallel}/PL_{\perp}$, was evaluated at 20.3 and 15.5 at 424 and 448 nm, respectively.

For the construction of the polarized OLEDs, indium tin oxide (ITO) coated glass substrates were treated with an oxygen plasma before applying a PEDOT/PSS conductive alignment layer followed by an oligo(fluorene) film, both by spin-coating. After the oligo(fluorene) layer was annealed as described above, the following layers were vacuum-deposited sequentially: 1,3,5-tri(phenyl-2-benzimidazolyl)benzene, TPBI, as the electron-transport layer which also blocks holes and excitons; lithium fluoride as the electron injection layer;[23] and magnesium/silver (20:1) as the cathode. The structure of the resulting OLED is depicted as the inset in Figure 3b. The oligo(fluorene) structure and its thickness were varied to permit an investigation of their effects on device performance. The polarized EL spectra at a current density of 20 mA cm^{-2} are displayed in Figure 3b in terms of the emission intensity parallel ($EL_{\parallel}$) and perpendicular ($EL_{\perp}$) to the nematic director for a 35 nm thick **F(MB)10F(EH)2** film. A comparison of Figures 3a,b reveals that the normalized photo- and electroluminescence spectra are nearly identical except the dichroic ratio. The EL dichroic ratio, $R_{EL} = EL_{\parallel}/EL_{\perp}$ was evaluated at 27.1 and 31.2 at 424 and 448 nm, respectively. The observed R_{EL} values were found to be independent of current density. Across the EL spectral range from 400 to 600 nm, the ratio of the integrated $EL_{\parallel}$ to $EL_{\perp}$ (i.e., the integrated dichroic ratio) was evaluated at 24.6 with a luminance yield of 1.07 cd A^{-1} measured without _polarization analysis. The deep blue emission from this device is indicated by the Commission Internationale de L'Eclairage (CIE) coordinates (0.159, 0.062). The relationships between _current density, applied voltage, and luminance, as shown for **F(MB)10F(EH)2** in Figure 3c, indicate a turn-on voltage which decreases with a decreasing film thickness (less than 5 V in both cases). Moreover, at 20 mA cm^{-2} the 35 and 73 nm film

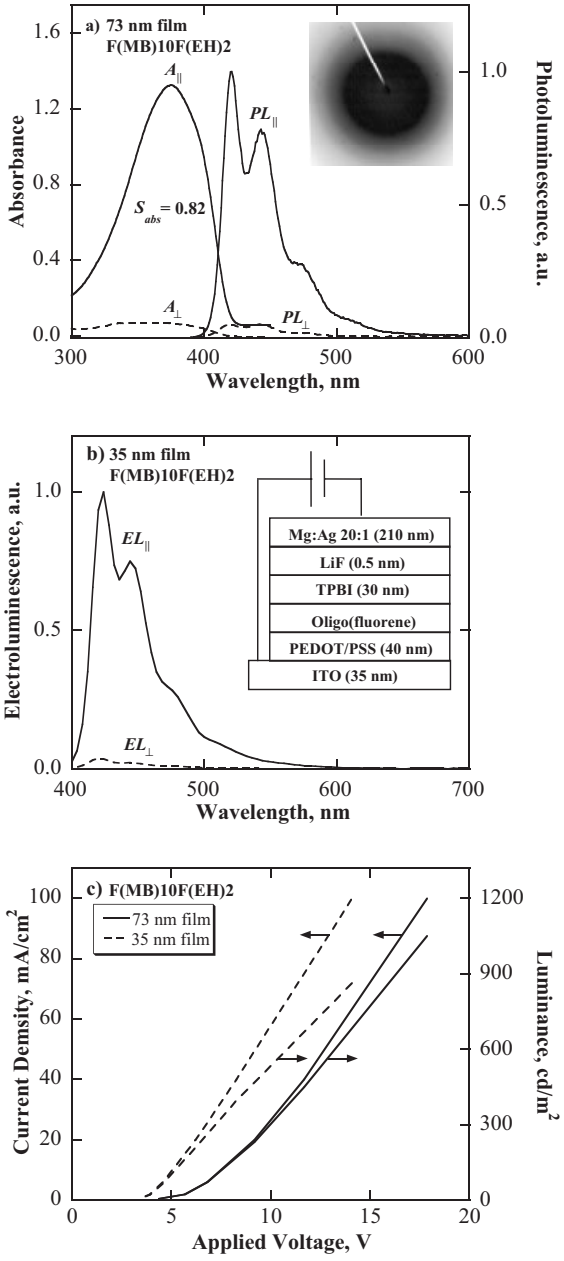

Fig. 3.a) Linearly polarized absorption and photoluminescence (with unpolarized excitation at 370 nm) spectra of an OLED containing a 73 nm thick **F(MB)10F(EH)2** film, with an inset showing the electron diffraction pattern; b) device structure and the polarized EL spectra for an OLED containing a 35 nm thick **F(MB)10F(EH)2** film at a current density of 20 mA cm^{-2}, and c) current density–applied voltage–luminance relationships for OLEDs containing a 35 and 73 nm thick **F(MB)10F(EH)2** films.

showed a luminance of 214 and 220 cd m^{-2} at 6.2 and 9.5 V, respectively.

The device features and performance data at 20 mA cm^{-2} for all the OLEDs prepared for the present study are compiled in Table 1. Within the **F(MB)10F(EH)2** series, the higher degree of uniaxial alignment achieved with the thinner films is manifested in the higher S_{ab} and R_{EL} values. This is probably due to the stronger surface anchoring provided by the buffed PEDOT/PSS conductive alignment layer. The driv-

Table 1. OLED device features and performance data at a current density of 20 mA cm^{-2}.

Device [a]	Annealing time [min]	Thickness [b] [nm]	S_{abs} [c]	Voltage [V]	Yield [cd/A]	R_{EL} [d] λ_1	λ_2	R_{EL} integrated	CIE (x,y)
				Dodecamer, **F(MB)10F(EH)2**					
A	60	73	0.82	9.5	1.10	17.3	15.4	14.4	(0.159,0.079)
B	60	48	0.84	6.4	0.97	13.3	19.4	15.3	(0.156,0.070)
C	30	35	0.88	6.2	1.07	27.1	31.2	24.6	(0.159,0.062)
				Heptamer, **F(Pr)5F(MB)2**					
D	30	70	0.80	7.2	0.98	14.7	10.5	11.7	(0.157,0.085)
				Pentamer, **F(MB)5**					
E	30	68	0.75	9.7	0.48	11.8	9.5	8.6	(0.159,0.091)

[a] Experimental uncertainties assessed with 5 sets of device A are as follows: film thickness, ±5 nm; orientational order parameter, ±0.01; drive voltage, ±0.2 V; yield, ±0.07 cd/A; emission peak dichroic ratios, ±0.7; integrated dichroic ratio, ±0.5; CIE coordinates, ±0.002. [b] Determined by variable angle spectroscopic ellipsometry. [c] Orientational order parameter determined from UV-vis linear dichroism. [d] Emission peak maxima at $\lambda_1 = 424$ and $\lambda_2 = 448$ nm, dodecamer; $\lambda_1 = 420$ and $\lambda_2 = 448$ nm, heptamer; and $\lambda_1 = 412$ and $\lambda_2 = 444$ nm, pentamer. [e] The EL spectra were integrated from 400 to 600 nm.

ing voltage decreases with a decreasing film thickness as expected, while the luminance yield remains constant within experimental uncertainties. With a comparable film thickness in devices A, D, and E (i.e., 73, 70, and 68 nm, respectively), both S_{ab} and R_{EL} values decrease with a decreasing chain length, consistent with the notion that the degree of uniaxial alignment is determined by molecular aspect ratio. Note that S_{ab} values of 0.82, 0.80, and 0.75 correspond to R_{ab} values of 14.7, 13.0, and 10.0, a trend consistent with the R_{EL} values reported in Table 1. The lower driving voltage in device D in comparison to A and E might have arisen from the higher charge carrier mobility through the heptafluorene film because of the less bulky pendant group. The lower efficiency observed for the pentamer device than the heptamer and dodecamer devices is likely due to a higher barrier to charge carrier injection. Of the five OLEDs presented in Table 1, the 35 and 48 nm thick films show a greater R_{EL} value at the lower energy emission peak than that at the higher energy peak, a trend opposite to that of the three thicker films. The CIE coordinates of all five OLEDs are closer to the National Television System Committee standard blue, viz. (0.14, 0.08), than previously reported polarized OLEDs using poly(fluorene)s.[10,13] Moreover, a luminance yield up to 1.10 cd A^{-1}, an emission peak dichroic ratio up to 31.2, and an integrated dichroic ratio up to 24.6 are all superior to prior reports using poly(fluorene)s. This set of performance data in a single device compares favorably with those achieved independently using poly(fluorene)s, such as an emission peak dichroic ratio of 25,[14] an integrated dichroic ratio of 21,[10] and a luminance yield of 0.66 cd A^{-1} with CIE coordinates of (0.17, 0.12).[13b] To elucidate the role played by the electron transport layer, an OLED with the configuration ITO/PEDOT/oligofluorene/LiF/Ca/Al[24] containing a 50 nm thick **F(MB)10F(EH)2** layer, was fabricated for comparison. This device showed a luminance yield of 0.18 cd A^{-1}, demonstrating the importance of TPBI for electron injection and carrier confinement in the emitting layer to achieve a high efficiency. To investigate the effects of molecular order on device performance, OLEDs equivalent to those reported in Table 1 were prepared without thermally annealing the oligofluorene films. The CIE coordinates and luminance yields of the essentially isotropic OLEDs were found to be similar to those observed for the aligned devices (see Table 1). This is in sharp contrast to poly(fluorene) based polarized OLEDs, in which thermal annealing often causes color instability with a diminished efficiency.[10,13b]

In summary, monodisperse glassy nematic oligo(fluorene)s were successfully employed for the fabrication of strongly polarized and efficient, deep blue OLEDs. The requisite uniaxial molecular alignment was accomplished by spin-casting oligo(fluorene)s onto a PEDOT/PSS conductive alignment layer with subsequent thermal annealing under relatively mild conditions. Superior chemical purity and ease of material processing into monodomain films resulted in the highest EL dichroic ratio ever observed in polarized OLEDs. Furthermore, the polarized OLEDs based on monodisperse oligo(fluorene)s showed a deeper blue emission with a higher luminance yield than those prepared with poly(fluorene)s. At roughly the same film thickness, the EL dichroic ratio increases with an increasing chain length because of the higher degree of uniaxial molecular alignment. For a given oligo(fluorene) sample, the thinner the film, the higher the EL dichroic ratio because of the stronger surface anchoring furnished by the conductive alignment layer. The EL dichroic ratio increases with a decreasing film thickness in the case of dodecafluorene with largely the same luminance yield.

Experimental

Procedures for the synthesis and purification of the oligo(fluorene)s used in this study have been reported elsewhere [21]. Thermotropic properties were characterized by differential scanning calorimetry (Perkin-Elmer DSC-7) in conjunction with hot-stage polarizing optical microscopy (DMLM, Leica, FP90 central processor and F82 hot stage, Mettler Toledo). Films for electron diffraction (JEM 2000 EX, JEOL USA) were spin-cast on single crystalline sodium chloride substrates and then floated off in a trough filled with deionized water for mounting onto copper grids. As a conductive alignment layer, an aqueous dispersion of PEDOT/PSS (Baytron P VP AI 4083, Bayer) was spin-coated at

ADVANCED MATERIALS

2500 rpm followed by drying at 120 °C for 30 min under argon before uniaxial buffing was performed. Oligo(fluorene) films were prepared by spin-coating from 0.25–0.80 wt.-%, UV-grade chloroform solutions at 4000 rpm to arrive at a varying film thickness after thermal annealing at 10 °C above T_g under argon. After consecutive depositions of TPBI and LiF at 0.4 and 0.1 nm s^{-1}, the cathode was applied by co-depositing magnesium and silver at 1.00 and 0.05 nm s^{-1}, respectively. Sublimation of all materials was conducted at a vacuum level of 10^{-6} torr or higher. After encapsulation in a dry nitrogen glove box, the OLEDs were characterized using a Keithley 2400 source/measure unit and a PhotoResearch PR650 spectroradiometer capable of polarization analysis. A UV-vis-NIR spectrophotometer (Lambda-900, Perkin-Elmer) with a linear polarizer (H'NPB, Polaroid) was used to characterize linear dichroism. Photoluminescence was characterized using a spectrofluorimeter (Quanta Master C-60SE, Photon Technology International) with a liquid light guide directing unpolarized excitation at 370 nm onto the sample film at normal incidence. Polarization analysis of both photo- and electroluminescence was performed using a pair of linear polarizers.

Received: February 2, 2003
Final version: March 25, 2003

[1] *Semiconducting Polymers: Chemistry, Physics and Engineering* (Eds: G. Hadziioannou, P. F. van Hutten), Wiley-VCH, Weinheim **2000**.
[2] J. H. Burroughes, D. D. C. Bradley, A. R. Brown, R. N. Marks, K. MacKay, R. H. Friend, P. L. Burn, A. B. Holmes, *Nature* **1990**, *347*, 539.
[3] M. D. McGehee, A. J. Heeger, *Adv. Mater.* **2000**, *12*, 1655.
[4] C. D. Dimitrakopoulos, P. R. L. Malenfant, *Adv. Mater.* **2002**, *14*, 99.
[5] P. Strohriegl, J. V. Grazulevicius, in *Handbook of Organic Conductive Molecules and Polymers* (Ed: H. S. Nalwa), Vol. 1, Wiley, Chichester **1997**, Ch. 11.
[6] S. R. Marder, B. Kippelen, A. K.-Y. Jen, N. Peyghambarian, *Nature* **1997**, *388*, 845.
[7] C. W. Tang, S. A. VanSlyke, *Appl. Phys. Lett.* **1987**, *51*, 913.
[8] a) T. Q. Nguyen, I. B. Martini, J. Liu, J. Schwartz, *J. Phys. Chem. B* **2000**, *104*, 237. b) J. Teetsov, D. A. Vanden Bout, *J. Phys. Chem. B* **2000**, *104*, 9378.
[9] a) D. Katsis, Y. H. Geng, J. J. Ou, S. W. Culligan, A. Trajkovska, S. H. Chen, L. J. Rothberg, *Chem. Mater.* **2002**, *14*, 1332. b) W.-L. Yu, J. Pei, W. Huang, A. J. Heeger, *Adv. Mater.* **2000**, *12*, 828. c) S. Setayesh, A. C. Grimsdale, T. Weil, V. Enkelmann, K. Müllen, F. Meghdadi, E. J. W. List, G. Leising, *J. Am. Chem. Soc.* **2001**, *123*, 946. d) G. Klärner, J.-I. Lee, M. H. Davey, R. D. Miller, *Adv. Mater.* **1999**, *11*, 115.
[10] T. Miteva, A. Meisel, W. Knoll, H.-G. Nothofer, U. Scherf, D. C. Müller, K. Meerholz, A. Yasuda, D. Neher, *Adv. Mater.* **2001**, *13*, 565.
[11] M. Grell, D. D. C. Bradley, M. Inbasekaran, E. P. Woo, *Adv. Mater.* **1997**, *9*, 798.
[12] M. Grell, W. Knoll, D. Lupo, A. Meisel, T. Miteva, D. Neher, H.-G. Nothofer, U. Scherf, A. Yasuda, *Adv. Mater.* **1999**, *11*, 671.
[13] a) D. Sainova, A. Zen, H.-G. Nothofer, U. Asawapirom, U. Scherf, R. Hagen, T. Bieringer, S. Kostromine, D. Neher, *Adv. Funct. Mater.* **2002**, *12*, 49. b) X. H. Yang, D. Neher, S. Lucht, H. Nothofer, R. Güntner, U. Scherf, R. Hagen, S. Kostromine, *Appl. Phys. Lett.* **2002**, *81*, 2319.
[14] K. S. Whitehead, M. Grell, D. D. C. Bradley, M. Jandke, P. Strohriegl, *Appl. Phys. Lett.* **2000**, *76*, 2946.
[15] M. Jandke, D. Hanft, P. Strohriegl, K. Whitehead, M. Grell, D. D. C. Bradley, *SPIE Proc.* **2001**, *4105*, 338.
[16] A. E. A. Contoret, S. R. Farrar, P. O. Jackson, S. M. Khan, L. May, M. O'Neill, J. E. Nicholls, S. M. Kelly, G. J. Richards, *Adv. Mater.* **2000**, *12*, 971.
[17] S.-W. Chang, A.-K. Li, C.-W. Liao, C.-S. Hsu, *Jpn. J. Appl. Phys.* **2002**, *41*, 1374.
[18] A. Meisel, T. Miteva, G. Glaser, V. Scheumann, D. Neher, *Polymer* **2002**, *43*, 5235.
[19] a) S. A. Carter, M. Angelopoulos, S. Karg, P. J. Brock, J. C. Scott, *Appl. Phys. Lett.* **1997**, *70*, 2067. b) L. B. Groenendaal, F. Jonas, D. Freitag, H. Pielartzik, J. R. Reynolds, *Adv. Mater.* **2000**, *12*, 481.
[20] R. E. Martin, F. Diederich, *Angew. Chem. Int. Ed.* **1999**, *38*, 1350.
[21] Y. H. Geng, S. W. Culligan, A. Trajkovska, J. U. Wallace, S. H. Chen, *Chem. Mater.* **2003**, *15*, 542.
[22] M. Schubert, B. Rheinländer, C. Cramer, H. Schmiedel, J. A. Woollam, C. M. Herzinger, B. Johs, *J. Opt. Soc. Am. A* **1996**, *13*, 1930.
[23] L. S. Hung, C. W. Tang, M. G. Mason, *Appl. Phys. Lett.* **1997**, *70*, 152.
[24] T. M. Brown, R. H. Friend, I. S. Millard, D. J. Lacey, J. H. Burroughes, F. Cacialli, *Appl. Phys. Lett.* **2001**, *79*, 174.

Deformation of Nanoscopic Polymer Structures in Response to Well-Defined Capillary Forces**

By *Mark P. Stoykovich*, *Heidi B. Cao*, *Kenji Yoshimoto*, *Leonidas E. Ocola*, and *Paul F. Nealey**

The mechanical properties of materials in micro- and nanoscopic systems are of critical importance in the processing, design, and application of microelectronic devices, microelectromechanical systems (MEMS), and nanoelectromechanical systems (NEMS). Few methods, however, are available to measure mechanical properties at the nanoscale. Nanoindentation,[1] lateral force microscopy,[2] dynamic atomic force microscopy (AFM),[3] frictional force microscopy (FFM),[4] and interfacial force microscopy (IFM)[5] have been used to determine the out-of-plane mechanical and adhesion properties of films and microscopic (but not nanoscopic) two- and three-dimensional (2D, 3D) structures. Quantitative measurements on nanoscopic features using such tools may be precluded by the size of the microprobe tips (usually greater than 50 nm in diameter) and coupling of the mechanical properties to the sampling volume,[5d,6] tip–sample interactions, and the rate of energy dissipation.[1b,3c] Consequently the application of nanoindentation, AFM, FFM, and IFM mechanical tests on sub-100 nm 2D and 3D structures is difficult. In recent years, on-wafer measurement techniques have been applied to the determination of the biaxial modulus, Young's modulus, Poisson ratio, and coefficient of thermal expansion of thin films,[7] but less progress has been made regarding the mechanical properties of 2D or 3D nanoscale features.[8] In this paper, we report on the design and implementation of test structures in which well-defined capillary forces act on micro- and nanoscopic polymer beams. We demonstrate that the deformation of the beams can be quantified with respect to the initial applied forces. In addition, we present strategies for using the test structures in combinatorial arrays to investigate the beam properties in a high-throughput and statistically robust manner. We anticipate that, with the development of appropriate patterning techniques and deformation models, the test struc-

[*] Prof. P. F. Nealey, Dr. H. B. Cao,[+] M. P. Stoykovich, K. Yoshimoto
Department of Chemical Engineering and Center for NanoTechnology
University of Wisconsin
Madison, WI 53706 (USA)
E-mail: nealey@engr.wisc.edu
Dr. L. E. Ocola[++]
Advanced Lithography Research
Agere Systems
Murray Hill, NJ 07974 (USA)
[+] Present address: Intel Corporation, Hillsboro, OR 97124, USA.
[++] Present address: Center for Nanoscale Materials, Argonne National Laboratory, Argonne, IL 60439, USA.

[**] This work is based in part on grants from the Semiconductor Research Corporation (2002-MJ-985), the NSF Nanoscale Interdisciplinary Research Team program (CTS-0210588), the Camille Dreyfus Teacher–Scholar Awards Program, Sematech, and Intel Corporation. The Center for NanoTechnology, University of Wisconsin-Madison, is supported in part by DARPA/ONR (N00014-97-1-0460). The authors thank Agere Systems for providing access to the electron-beam lithography tool and related facilities.

  DOI: 10.1002/adma.200305059